HAL
open science

Shear strength and microstructure of 3D assemblies of platy particles

Mauricio Boton, Emilien Azéma, Nicolas Estrada, Farhang Radjai, Arcesio Lizcano

To cite this version:

Mauricio Boton, Emilien Azéma, Nicolas Estrada, Farhang Radjai, Arcesio Lizcano. Shear strength and microstructure of 3D assemblies of platy particles. Powder and Grains 2013, 2013, Sydney, Australia. pp.519-522. hal-00842787

HAL Id: hal-00842787

https://hal.science/hal-00842787v1

Submitted on 9 Jul 2013

HAL is a multi-disciplinary open access archive for the deposit and dissemination of scientific research documents, whether they are published or not. The documents may come from teaching and research institutions in France or abroad, or from public or private research centers.

L'archive ouverte pluridisciplinaire **HAL**, est destinée au dépôt et à la diffusion de documents scientifiques de niveau recherche, publiés ou non, émanant des établissements d'enseignement et de recherche français ou étrangers, des laboratoires publics ou privés.

Shear strength and microstructure of 3D assemblies of platy particles

Mauricio Boton[*,†], Emilien Azéma[†], Nicolas Estrada[*], Farhang Radjaï[†] and Arcesio Lizcano[**]

[*]*Departamento de Ingeniería Civil y Ambiental, Universidad de Los Andes, Bogotá, Colombia*
[†]*LMGC, Université Montpellier 2, CNRS, Place Eugène Bataillon, 34095 Montpellier cedex 05, France*
[**]*SRK Consulting (Canada) Inc., Vancouver, BC, V6E 3X2, Canada*

Abstract. As a first step towards particle-scale modeling of clayey soils, we investigate the mechanical behavior and microstructure of assemblies of three-dimensional rectangular platy particles by means of the discrete element method. Several samples composed of particles of different levels of platyness (ratio of width to thickness) were numerically prepared and sheared to large deformations. We analyze the shear strength, packing fraction, connectivity, contact and force anisotropies, and mobilization of friction forces as functions of platyness. We find that both the mechanical behavior and microstructure are strongly dependent on the degree of platyness. This happens, in particular, because of the alignment of particle faces along a particular direction. Additionally, as observed for other granular materials with complex shapes, the packing fraction passes by a peak value before decreasing for larger values of platyness.

Keywords: DEM, Clays, Microstructure, Shear strength
PACS: 0218

INTRODUCTION

The application of DEM to the study of soils has been restricted to a class of soils: *coarse soils*. Soils not belonging to this class (i.e., *fine soils*, such as clays) have been left out of the scope of this analysis tool, because a meaningful DEM simulation of a clayey soil should include, at least, three characteristics: (1) a complex particle shape, (2) a complex interaction between particles, and (3) a complex interaction between the particles and the fluid filling the voids between them. The implementation and the efficient treatment of these characteristics in a DEM simulation platform are difficult technical problems, which is why studies related to this subject are scarce [1, 2, 3, 4].

The aim of this work was to explore the effect of the platy shape of particles—typically observed in clay particles—on the mechanical behavior and the microstructure of a granular material using DEM. It is important to note that our strategy was to single out the effects of one of the distinctive characteristics of these materials, the shape of their particles, and to isolate this effect from those of other characteristics such as the complex particle-particle or particle-fluid interactions.

The effect of the platy shape of particles is evaluated by the platyness of the particles. The platyness, quantified through the parameter η, was varied systematically from $\eta = 0$, which corresponds to spherical particles, to $\eta = 0.8$, which corresponds to particles in which are 5 times longer than they are thick. Several monodisperse assemblies were numerically built, one for each value of η, and then sheared in the quasistatic limit up to the steady state, also called "critical state" in soil mechanics. In this state, we analyzed the mechanical behavior of the material at the macroscale, in terms of shear strength and solid fraction, as well as its microstructure, in terms of orientation of the particles, connectivity, fabric of the interactions network, and interaction forces.

NUMERICAL MODEL

We employed the Molecular Dynamics method, adapted by Cundall and Strack for simulating granular materials [5]. The particles were squared plates with rounded edges, built through a spheroplates (i.e., the shape resulting from sweeping a sphere around a square plate by means of a Minkowsky addition [6, 7, 8]). By definition, one spheroplate is composed of next entities: four vertices, four edges, and one face, see Fig. 1(a). The platyness η of these spheroplates was defined as $\eta = (R-r)/R$, where R and r are, respectively, the maximum and minimum radii of the spheroplate as defined in Fig. 1(b) (r is also called the spheroradius of the spheroplate).

In our system, one interaction ξ between two spheroplates represents single or multiple contacts c, each contact occurring between two entities belonging to either spheroplates. All possible contacts were resolved by considering two cases: a contact between two edges and a

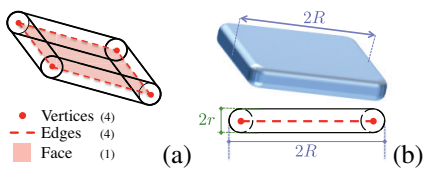

FIGURE 1. Color online. (a) Scheme of a spheroplate and its constitutive entities. (b) Definition of the maximum and minimum radii, R and r respectively.

contact between a vertex and a face [9].

Ten monodisperse made up of 8000 spheroplates were built. The spheroplates' platyness of the samples varied from $\eta = 0$ to 0.8. The spheroradius $r = 30$nm was the same for all samples, and the density ρ was 2700kg/m^3. The stiffness coefficients were 1.5×10^{-3}N/μm, and the damping coefficients were calibrated in order for the mechanical behavior to be independent of them. The friction coefficient μ was $0.58 \simeq \tan(30°)$, which is close to that of kaolinite clay. The samples were sheared up to a large cumulative shear strain $\gamma \simeq 2.5$ by imposing a constant velocity v_w and a confining stress σ_w to the upper wall. In all simulations presented in this work the gravity was set to zero. It was verified that all packings reached the steady state, since, at the end of the shear test, q/p fluctuated around mean values and the shear strain was uniformly distributed in the bulk. The quasistaticity of the simple shear tests and the stiffness of the particles was evaluated, respectively, with two dimensionless parameters [10, 11]: the inertia parameter $I \approx 10^{-3}$ and the dimensionless stiffness $\kappa > 10^3$. All presented quantities correspond to the average over the last 40% of cumulative shear strain (i.e., from $\gamma = 1.5$ to 2.5).

MECHANICAL BEHAVIOR

We analyze both stresses and strains in the steady state, in terms of shear strength and solid fraction. The shear strength was calculated from the stress tensor $\boldsymbol{\sigma}$ [12], defined as $\boldsymbol{\sigma} = (1/V)\sum_{\xi \in V}(F^{\xi}_{\alpha}\ell^{\xi}_{\beta})$, where V is the volume containing the interactions ξ, $\boldsymbol{F}$ is the interaction force, $\boldsymbol{\ell}$ is the branch vector (i.e., the vector joining the centers of the interacting particles), and α and β denote de components in the reference frame. The mean $p = (\sigma_1 + \sigma_3)/2$ and deviatoric $q = (\sigma_1 - \sigma_3)/2$ stresses were then calculated from the principal stresses σ_1 and σ_3. We decided to exclude the intermediate principal stress σ_2 from the calculation of p and q, since the simple shear test implies plane strain conditions. The shear strength of the material can be expressed as the stress ratio q/p, see Fig. 2. We can see that q/p increases almost linearly with η, approximately from 0.3 to 0.7, showing that, as the particles' platyness increases, the material's shear strength also increases.

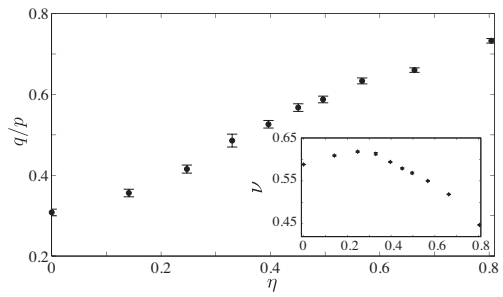

FIGURE 2. Shear strength q/p as a function of the platyness η. The inset shows the solid fraction ν as a function of η. Error bars indicate the standard deviation.

On the other hand, the solid fraction is defined as $\nu = V_p/V$, where V_p is the volume occupied by the particles and V is the total volume. We can see that ν first increases with η, then reaches a maximum at $\eta \simeq 0.3$, and then declines as η increases. This shows that the relationship between the platyness of the particles and the material's solid fraction is not monotonic.

MICROSTRUCTURE

We analyze the microstructure of the samples in terms of particles' orientation, connectivity, fabric of the interactions network, and interaction forces. Because of the symmetry of our simple shear tests, we analyzed all quantities and results in the xy plane. First, the particles' orientation was defined as the orientation of the vector $\boldsymbol{m}$, which is normal to the particle face. The distribution of particle orientations can be represented by the probability density function $P_m(\theta)$ of particles whose vector $\boldsymbol{m}$ is oriented along a direction close to a angle θ. Then, $P_m(\theta)$ can be approximated by its lowest order Fourier expansion: $1/\pi[1 + a_m \cos 2(\theta - \theta_m)]$, where a_m is the anisotropy of particle orientations and θ_m is the principal direction of $P_m(\theta)$. Figure 3 shows the anisotropy of particle orientations a_m and the principal direction θ_m as functions of the platyness η. We can see that a_m increases almost linearly from 0 to approximately 0.6, showing that, as the particles' platyness increases, the number of particles aligning their faces along a particular direction increases. Following an opposite trend, θ_m decreases with η, approximately from 120° to 105°, showing that, as the particles' platyness increases, the direction along which these particles align gradually approaches the vertical direction. Note that this kind of ordering appears even in the samples made up of particles with very low values of η (e.g., for $\eta = 0.14$), whose shape deviates only slightly from that of a sphere.

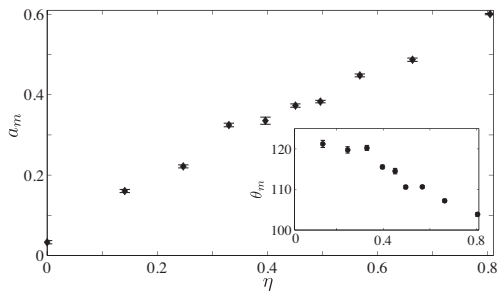

FIGURE 3. Anisotropy of particle orientations a_m as a function of the platyness η. The inset shows the principal direction θ_m as a function of η.

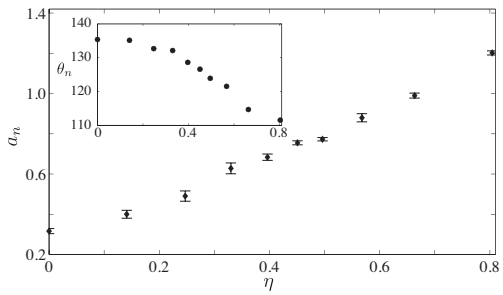

FIGURE 5. Anisotropy of interaction orientations a_n as a function of the platyness η. The inset shows the principal direction θ_n as a function of η.

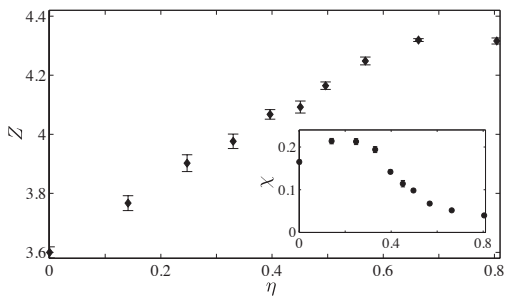

FIGURE 4. Coordination number Z as a function of the platyness η. The inset shows the proportion χ of floating particles as a function of η.

Figure 4 shows the coordination number Z as a function of the platyness η. Remark that Z is the mean number of interactions per particle, where an interaction can comprise several contacts. We can see that Z increases with η, approximately from 3.6 to 4.3, and stabilizes for the larger values of η. This shows that, as the particles' platyness increases, the material's connectivity also increases. This is a somehow a counterintuitive result, since, as it was shown in the inset of Fig. 2, these very connected samples are also the loosest ones. The inset on Fig. 4 shows the proportion χ of floating particles as a function of the platyness η. We can see that χ decreases with η, approximately from 0.20 to 0.05. This shows that, as the particles' platyness increases, the number of particles participating in the force carrying network also increases. This explains the increase in coordination as a function of platyness.

The fabric of the interactions network can be represented by the probability density functions $P_n(\theta)$ of interactions whose normal $\boldsymbol{n}$ is oriented along a direction close to a angle θ. Then, $P_n(\theta)$ can be approximated by its lowest order Fourier expansion: $1/\pi[1+a_n\cos 2(\theta-\theta_n)]$, where a_n is the anisotropy of interaction orientations and θ_n is the principal direction of $P_n(\theta)$. Figure 5 shows the anisotropy of interaction orientations a_n and the principal direction θ_n as functions of the platyness η. We can see that a_n increases almost linearly with η, approximately from 0.3 to 1.2, showing that, as the particles' platyness increases, the number of interactions aligning along a particular direction also increases. Then, as observed for θ_m, θ_n decreases with η, approximately from 135° to 110°, showing that, as the particles' platyness increases, the direction along which these interactions align gradually approaches the vertical direction. These similarities between the parameters describing the distributions $P_m(\theta)$ and $P_n(\theta)$ are to be expected, since, by construction, the vectors $\boldsymbol{m}$ and $\boldsymbol{n}$ are correlated in interactions involving the particles faces, and, as the particles platyness increases, the proportion of this kind of interactions is expected to increase.

The interaction force $\boldsymbol{F}$ between two particles was calculated by adding the forces $\boldsymbol{f}$ exerted at each contact point. As $\boldsymbol{f}$, $\boldsymbol{F}$ can be decomposed in the normal and tangential directions: $\boldsymbol{F}=F_n\boldsymbol{n}+F_t\boldsymbol{t}$. The distributions of interaction forces can be represented by $\langle F_n\rangle(\theta)$ and $\langle F_t\rangle(\theta)$, which are, respectively, the distributions of average interaction forces in the normal and tangential directions. By construction, F_n is always positive, while F_t can take positive or negative values. Then, $\langle F_n\rangle(\theta)$ and $\langle F_t\rangle(\theta)$ can be approximated by their lowest order Fourier expansions: $\langle F_n\rangle(\theta)=\langle F_n\rangle[1+a_{fn}\cos 2(\theta-\theta_{fn})]$ and $\langle F_t\rangle(\theta)=\langle F_n\rangle a_{ft}\sin 2(\theta-\theta_{ft})$, where a_{fn} and a_{ft} are, respectively, the anisotropies of normal and tangential interaction forces, and $\theta_{fn}\simeq\theta_{ft}$ are, respectively, the principal directions of $\langle F_n\rangle(\theta)$ and $\langle F_t\rangle(\theta)$.

Figure 6 shows the anisotropies of normal and tangential interaction forces, a_{fn} and a_{ft} respectively, as well as the principal direction θ_{fn}, as functions of the platyness η. Firstly, we can see that a_{fn} increases slowly with η, approximately from 0.2 to 0.3. This shows that the particles' platyness has little effect on the magnitude of the normal forces transmitted between particles. Secondly, we can see that a_{ft} increases with η, approximately from 0.05 to 0.7. This shows that, as the particles' platyness increases, the magnitude of the tangen-

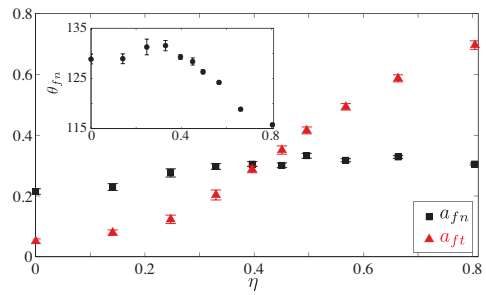

FIGURE 6. Color online. Anisotropies of normal (black) and tangential (red) interaction forces, a_{fn} and a_{ft} respectively, as functions of the platyness η. The inset shows the principal direction θ_{fn} as a function of η.

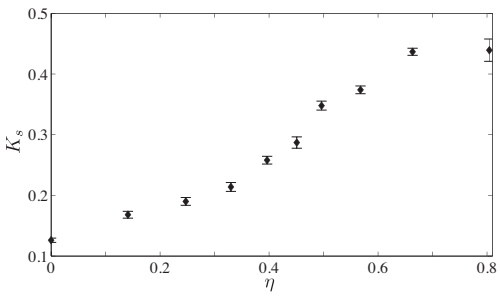

FIGURE 7. Proportion of sliding interactions K_s as a function of η.

tial forces transmitted between particles also increases. Thirdly, we can see that, as observed for θ_m, θ_n, and θ_{ln}, θ_{fn} decreases with η, approximately from 130° to 115°, showing that, as the particles' platyness increases, the direction along which the largest normal forces are transmitted, gradually approaches the vertical direction; the direction along which the largest tangential forces are transmitted is shifted by approximately 45°.

The slow increase of the anisotropy of normal interaction forces a_{fn} and the fast increase of the anisotropy of tangential interaction forces a_{ft} with the platyness η suggest that as the particles' platyness increases the stability of the interactions depends more and more strongly on friction forces. At the lowest order, this can be easily quantified by considering the proportion K_s of "sliding" interactions (i.e., those interactions in which $F_t/F_n \simeq \mu$). Figure 7 shows K_s as a function of η. It can be seen that K_s increases with η, approximately from 0.1 to 0.4. This shows that, as the particles' platyness increases, the level of friction mobilization, which reflects de dependence of the mechanical stability of the material on friction forces, also increases. The relationship between particle shape and friction mobilization seems to be a robust feature of granular materials made up of complex particles.

CONCLUSION

Firstly, we found that the mechanical behavior at the macroscale is strongly dependent on the particle platyness. On the one hand, the shear strength increases almost linearly with the platyness, and, on the other hand, the packing fraction first increases to a peak and then declines as the platyness further increases. Secondly, from the micromechanical point of view, we found that the principal phenomenon underlying the effects of the particles' platyness is the alignment of particle faces along a particular direction. In fact, all descriptors of the microstructure studied in this work are strongly influenced by this ordering phenomenon, showing that platyness, through this phenomenon, enhances the ability of the system to generate anisotropic structures. A direct consequence of this anisotropic structure is the large shear strengths measured in the materials composed of very platy particles.

ACKNOWLEDGMENTS: This work was financially supported by the *Centro de Estudios Interdisciplinarios Básicos y Aplicados en Complejidad (CEIBA)*.

REFERENCES

1. A. Anandarajah, *Powder Technology* **106**, 132 – 141 (1999), ISSN 0032-5910.
2. A. Anandarajah, *Computers and Geotechnics* **27**, 1 – 17 (2000), ISSN 0266-352X.
3. A. Anandarajah, *Computers and Geotechnics* **27**, 1 – 17 (2000), ISSN 0266-352X.
4. M. Yao, and A. Anandarajah, *Journal of Engineering Mechanics* **129**, 585–596 (2003).
5. P. A. Cundall, and O. D. L. Strack, *Géotechnique* **29**, 47–65 (1979).
6. L. Pournin, M. Weber, M. Tsukahara, J.-A. Ferrez, M. Ramaioli, and T. M. Liebling, *Granular Matter* **7**, 119–126 (2005), ISSN 1434-5021, 10.1007/s10035-004-0188-4.
7. S.-A. Galindo-Torres, F. Alonso-Marroquín, and Y. Wang (2008), `arXiv/0811.3060`.
8. F. Alonso-Marroquín, *EPL (Europhysics Letters)* **83**, 14001 (2008).
9. J. Ghaboussi, and R. Barbosa, *International Journal for Numerical and Analytical Methods in Geomechanics* **14**, 451–472 (1990), ISSN 1096-9853.
10. G. MiDi, *The European Physical Journal E* **14**, 341–365 (2004).
11. F. Radjai, F. Dubois, and F. Dubois, *Discrete-Element Modeling of Granular Materials*, John Wiley & Sons, 2011, ISBN 9781848212602.
12. J. J. Moreau, "Numerical Investigation of Shear Zones in Granular Materials," in *Friction, Arching, Contact Dynamics*, edited by D. E. Wolf, and P. Grassberger, World Scientific, Singapore, 1997, pp. 233–247.